Open Access

Journal of Energy and Power Technology

LIDSEN Publishing Inc.

Research Article

Electrochemical Synthesis of Germanium-Polypyrrole Composite Nanomaterials in Ionic Liquids for the Fabrication of Lithium-Ion Batteries

Zhen Liu [1,*], Li Yang [1], Abhishek Lahiri [2], James F Rohan [3], Frank Endres [1,*]

1. Institute of Electrochemistry, Clausthal University of Technology, Arnold-Sommerfeld-Strasse 6, 38678 Clausthal-Zellerfeld, Germany; E-Mails: zhen.liu@tu-clausthal.de; li.yang@tu-clausthal.de; frank.endres@tu-clausthal.de
2. Department of Chemical Engineering, Brunel University London, Kingston Lane, Uxbridge UB8 3PH, Middlesex, England; E-Mail: abhishek.lahiri@brunel.ac.uk
3. Electrochemical Materials and Energy Group Tyndall National Institute, University College Cork, Lee Maltings, T12 R5CP Cork, Ireland; E-Mail: james.rohan@tyndall.ie

* **Correspondence:** Zhen Liu and Frank Endres; E-Mails: zhen.liu@tu-clausthal.de; frank.endres@tu-clausthal.de

Academic Editor: Ahamed Irshad

Special Issue: Batteries: Past, Present and Future

Journal of Energy and Power Technology
2022, volume 4, issue 1
doi:10.21926/jept.2201010

Received: December 26, 2021
Accepted: March 15, 2022
Published: March 27, 2022

Abstract

Herein, we report the coating of nanostructured germanium using a polypyrrole (PPy) polymer coat as a composite anode material for the fabrication of lithium-ion batteries. The Ge/PPy composites were synthesized following the direct electrochemical deposition method in an ionic liquid (IL). The results revealed that the coating of PPy on Ge helped realize stable battery cycling and reversible capacities, which were not observed in uncoated Ge. The PPy layers could effectively inhibit side reactions between the electrode and electrolyte. The composition of the solid electrolyte interphase (SEI) formed after lithiation/delithiation cycles were analyzed using the X-ray photoelectron spectroscopy (XPS). Compact SEI layers consisted of decomposed $TFSI^-$ anion products such as LiF, Li_2S, $Li_2NS_2O_4$, and Li_2CO_3 at the Ge-PPy/IL interphase. In contrast, thick SEI layers consisted of not only decomposed $TFSI^-$ anion and

$[Py_{1,4}]^+$ cation products but also chemically or physically adsorbed IL compounds at the Ge/IL interphase. In addition, the PPy coating could effectively inhibit Ge oxidation, resulting in improved battery capacity.

Keywords
Ionic liquid; germanium; Polypyrrole; Li-ion battery; SEI; XPS

1. Introduction

Lithium-ion batteries (LIBs) are widely used in portable devices, electric vehicles, and grid-scale stationary energy storage systems [1-3]. However, the low theoretical capacity of traditional graphite anode limits its capacity [4]. Other group IV element-based anode materials, such as silicon (Si) and germanium (Ge), exhibit significantly high lithium-ion storage capacities [5-6]. Therefore, they are regarded as promising alternatives to commercial graphite anodes that are used for the fabrication of LIBs. The capacity of Ge (theoretical capacity: 1384 mAh g^{-1}) is less than the capacity of Si (3579 mAh g^{-1}). It is more expensive than Si [7-9]. However, Ge is still a promising anode material for high-power LIBs, as its conductivity is 10^4 times higher than the capacity of Si. Li ions diffuse 400 times faster in Ge than in Si at room temperature (~20 °C)[10-12].

A significant change in the volume of Ge during lithiation and delithiation has been observed, and this results in severe pulverization [13]. The development of nanostructured Ge such as nanoparticles, nanowires, and nanotubes could improve the battery performance as those nanomaterials can adjust to the volume changes without significant loss of structural integrity [14-20]. However, Ge nanomaterials tend to merge into micrometer-sized particles during the Li-ion insertion/extraction processes [21]. Therefore, thin and robust solid electrolyte interphase (SEI) layers are needed to stabilize the interphase [22]. However, it has been observed that the SEI layers crack during cycling. The Ge anode gets exposed to the electrolyte, resulting in the growth of SEI and oxidation of the anode material. This decreases the battery performance over time. It was revealed that a stable SEI layer could be formed on graphite anodes using carbonate electrolytes (such as ethylene carbonate (EC), dimethyl carbonate (DMC), and diethyl carbonate (DEC)). The layer could not be formed on Ge anodes [23]. It has also been reported that fluoroethylene carbonate (FEC) can effectively stabilize the Ge/electrolyte interphase and improve battery cycling [9]. FEC is less susceptible to oxidation, and the reduction of FEC results in the generation of fluoride ions and the formation of LiF, which in turn results in the formation of a relatively stable SEI layer [24-25].

Recently, polypyrrole (PPy), such as SnO_2-PPy [26], CoP_3@PPy [27], and α-Fe_2O_3/PPy [28], have been used as additives for the fabrication of anodes used in lithium-ion batteries to improve the battery cycling performance. The introduction of conductive polymers on Ge was also reported to be an effective method to stabilize the SEI layer as the polymer could buffer the volume changes during the cycling process [4, 29-30]. Inspired by these findings, we have fabricated PPy-coated nanostructured Ge composite electrodes.

The process of synthesis of nanostructured Ge is normally expensive and complicated, and this limits the use of Ge-based electrodes. Therefore, the electrodeposition of Ge thin film has gained

immense interest, as it is a low-cost method. Due to their limited electrochemical window, aqueous solutions are not suitable for the realization of Ge electrodeposition [31]. The electrodeposition of Ge thin film (from organic solutions) also showed low current efficiency, and this could be attributed to the evolution of hydrogen during the deposition process [32-33]. To address the problem posed by the evolution of hydrogen, ionic liquids (ILs) were used as solvents for Ge deposition.

We introduce the process of fabrication of PPy coated nanostructured Ge composite electrodes. The fabrication process was realized following a simple two-step electrodeposition process in 1-butyl-1-methylpyrrolidinium bis(trifluoromethylsulfonyl)imide ([$Py_{1,4}$]TFSI) ionic liquid. The obtained Ge-PPy composite electrode could be used as an anode material in fluorine-containing IL electrolytes. The electrochemical performance and the composition of the Ge-PPy/IL electrolyte interphase were investigated. The Ge/IL and the Ge/PVdF-HFP-IL polymer gel electrolyte interphases, formed during lithiation/delithiation processes, were also studied.

2. Materials and Methods

2.1 Electrodeposition of Ge from an Ionic Liquid Electrolyte

The ionic liquid 1-butyl-1-methylpyrrolidinium bis(trifluoromethylsulfonyl)imide, [$Py_{1,4}$] TFSI, was purchased in its most pure form from Io-Li-Tec (Germany). It was used after drying under a vacuum at 100 °C. The water content was reduced to < 2 ppm (Metrohm, Germany). $GeCl_4$ (99.9%; 0.2 mol/L) was purchased from Alfa Aesar. The electrochemical cell was made of Teflon and clamped over a Teflon-covered Viton O-ring onto the substrate, yielding a geometric surface area of 0.3 cm^2. The Teflon cell and the O-ring were cleaned using a mixture of concentrated H_2SO_4 and H_2O_2 (35%) (50:50, vol%). Subsequently, the sample was refluxed in distilled water. The working electrode in the experiment was a copper plate. Prior to conducting the experiments, the copper plate was cleaned using isopropanol and acetone to remove surface contaminants. Platinum wires were used as the counter and quasi-reference electrodes. For germanium deposition, a constant potential deposition method was conducted for 30 min in an argon-filled glove box. The water and oxygen contents were < 2 ppm (OMNI-LAB from Vacuum Atmospheres). Following electrodeposition, the residual ionic liquid in the cell was removed, and the electrodeposited germanium was cleaned using the pure ionic liquid kept inside the glove box.

2.2 Germanium-Polypyrrole (PPy) Composite Anode

The PPy films were coated onto the electrodeposited Ge following the process of anodic oxidation of pyrrole in the [$Py_{1,4}$]TFSI electrolyte (concentration: 0.05 mol/L pyrrole/IL). To be specific, a three-electrode cell was used to conduct the oxidation experiment. Cu, electrodeposited with Ge, was used as the working electrode. Pt wires were used as reference and counter electrodes. The PPy film was grown potentiostatically at 0.5 V vs. Pt for 30 min. Following the deposition process, the PPy-coated Ge electrode was washed thrice with acetone.

2.3 Ionic Liquid-Polymer Gel Electrolyte

The ionic liquid electrolyte for the battery test was prepared by dissolving 1 mol/L of LiTFSI in [$Py_{1,4}$]TFSI. The polymer poly (vinylidenefluoride hexafluoropropylene) (PVdF-HFP) was dissolved in acetone. The weight of the polymer was 7.5 wt.%. Subsequently, the ionic liquid was mixed with the

PVdF-HFP/acetone solution and stirred magnetically over a period of 30 min. The weight ratio of the ionic liquid electrolyte to PVdF-HFP was at 7:3. Thereafter, the solution was poured into a small evaporation pan and dried at 60 °C in a vacuum for 4 h to allow the evaporation of acetone.

2.4 Assembling the Cell and Cell Characterization

The sandwich cell consisted of a metallic Li electrode, a glass fiber separator, and a Ge or a Ge-PPy composite electrode. The mass loading corresponding to the active materials was ~5.2 mg/cm^2. The charge--discharge profiles were studied on a battery test instrument (Arbin BT2000, USA). The electrochemical measurements were performed using a VersaStat II (Princeton Applied Research, USA) potentiostat/galvanostat controlled by powerCV and power-step software. The obtained deposits were characterized using the scanning electron microscopy (SEM, JSM 7610F, JEOL, Japan) technique. The X-ray Photoelectron Spectroscopy (XPS) technique was used for sample analysis and a Specs Phoibos 150 hemispherical analyzer equipped with a Specs XR50 M monochromatic Al Kα source (1486.6 eV) with a base pressure of < 5 × 10^{-10} bar (SPECS, Germany) was used to conduct the experiments.

3. Results

3.1 Synthesis and Characterization of the PPy Coated Ge

Figure 1a presents the results obtained using the cyclic voltammetry (CV) technique. $GeCl_4$/[$Py_{1,4}$]TFSI (0.2 M) was used to study the Cu substrate in the cathodic regime at a scan rate of 10 mV/s. The electrode potential was scanned starting from the open circuit potential (OCP) in the negative direction. The presence of two significantly intense reduction peaks was observed. The first peak appearing at −1.7 V was attributed to the reduction of Ge(IV) to Ge(II), and the second peak at −2.2 V was attributed to the reduction of Ge(II) to Ge(0) [12]. Chronoamperometry experiments were performed to understand the reduction and growth mechanisms of Ge. The current density vs. time profile recorded at a potential of −2.2 V (recorded over 30 min) is shown in Figure 1b. A charged double-layer formed at the electrolyte/electrode interface in the presence of applied voltage. The sudden increase in the current was attributed to the formation and growth of the nuclei on the substrate. The nuclei continued to grow until the maximum current was attained [34, 35]. The concentration gradient resulted in a rapid decrease in the cathodic current density within a short time. Subsequently, the current density became stable, and the growth of the Ge nuclei was controlled via a diffusion process.

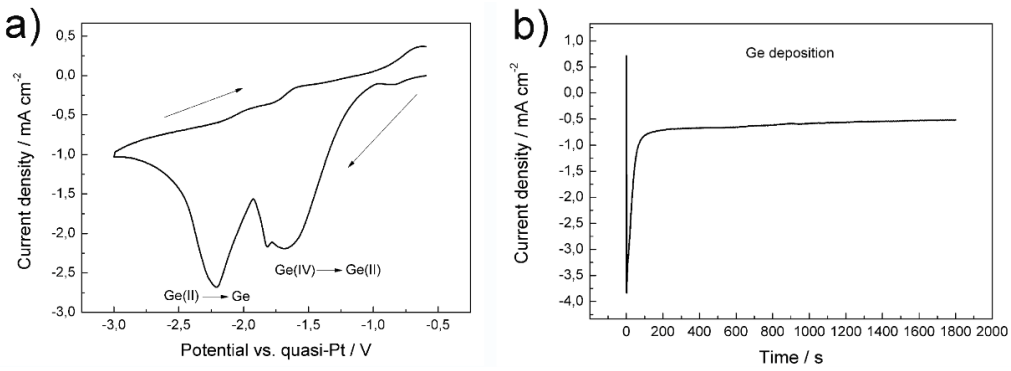

Figure 1 a) Cyclic voltammetry measurements for 0.2 mol/L $GeCl_4$/[$Py_{1,4}$]TFSI on Cu. The scan rate was 10 mV s^{-1}, b) Chronoamperogram used to analyze 0.2 mol/L of $GeCl_4$/[$Py_{1,4}$]TFSI (on Cu) at a potential of −2.2 V (time: 30 min).

The SEM images with different magnifications of the Ge deposits obtained by electrodeposition at −2.2 V for 30 min are shown in Figures 2a and 2b. The diameters of the grains are in the range of a few micrometers and form a more or less compact film. Figure 2b revealed that the pristine Ge particle was with diameter approximately 300 nm and these particles clustered into large agglomerates. The Ge deposit was washed thrice with acetonitrile and transferred directly from the glove-box to the XPS chamber. Contact with air was avoided. Analysis of the XPS survey spectral profile revealed that only Ge was present on the surface, and oxidized products were absent. The elemental Ge 2p 3/2 peak appeared at 1217.6 eV, which was typical for Ge (0). This indicated that high-quality Ge was prepared.

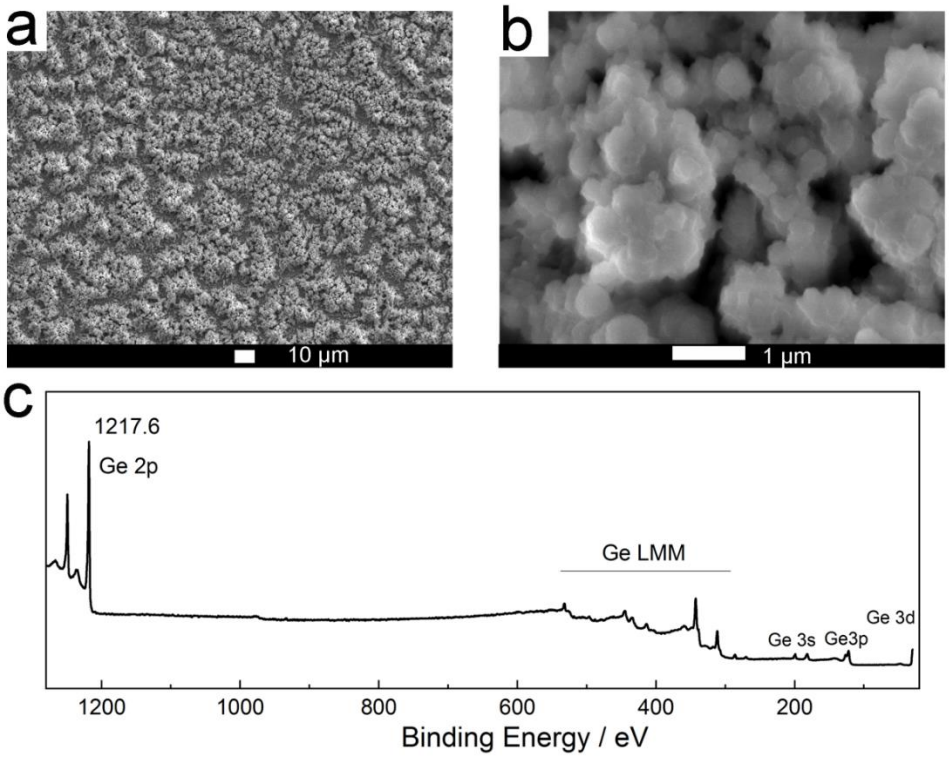

Figure 2 a) and b) SEM images with different magnifications of the electrodeposited Ge obtained at −2.2 V over a period of 30 min; c) XPS survey profiles recorded for the Ge deposits.

The morphological features of the PPy-coated Ge are presented in Figures 3a and 3b. Analysis of the SEM image of the PPy coatings (Figure 3a) reveals the presence of micrometer-sized particles that were uniformly distributed on the Ge surface. The surface morphology presented in Figure 3b shows that the polypyrrole films consist of cauliflower-like structures. The EDX patterns in the inset of Figure 3a present peaks corresponding to C, Ge, and Cu. The residual electrolyte on the surface contributes to the generation of the Cl, F, S, and O peaks. The XPS results also show the presence of residual ionic liquid. Analysis of the high-resolution N 1s spectral profile revealed that PPy was successfully coated onto Ge. The XPS profile recorded for $[Py_{1,4}]TFSI$ shows the presence of two N 1s peaks. The one at the higher binding of 403.1 eV was attributed to the $[Py_{1,4}]^+$ cation, and the one at a lower binding energy of 400 eV was assigned to the $TFSI^-$ anion [36]. The area ratio of the two peaks should be roughly 1:1. In this case, the N 1s peak at 400 eV has a much higher integrated area than that at 403.1 eV, suggesting that the N 1s of PPy contributes to the peaks at 400 eV.

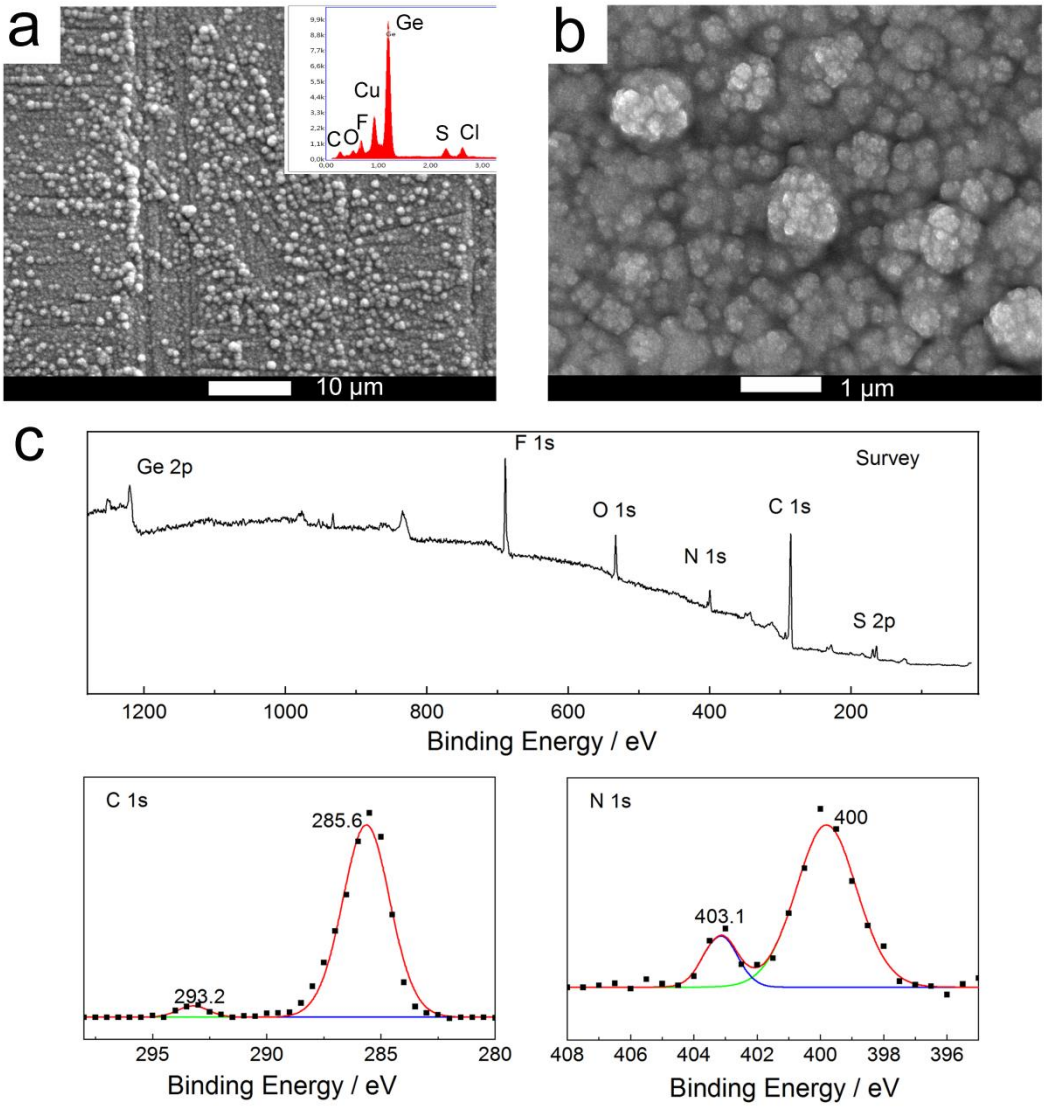

Figure 3 a) and b) Morphologies of the PPy-coated Ge deposits; c) XPS survey profiles and the detailed C 1s and N 1s profiles of the Ge-PPy composite.

3.2 Electrochemical Performance of the Electrode

The electrochemical performances of Ge and Ge-PPy anodes for LIBs were subsequently investigated by conducting lithiation and delithiation cycles using the cyclic voltammetry technique. The cyclic voltammograms recorded for 1 mol/L LiTFSI-[$Py_{1,4}$]TFSI on Ge and Ge-PPy substrates are depicted in Figure 4. In both cases, the cyclic voltammograms recorded during the first cycle differ from those recorded in subsequent cycles. In the first cycle, two reduction peaks at 1.75 V and 0.85 V were observed, which could be attributed to the formation of SEI. In the subsequent cycles, a redox couple appeared at 0.45 V and 0.6 V, as indicated by the red arrow in Figure 4, and this could be attributed to the intercalation of Li and the formation of the Li_xGe alloys.

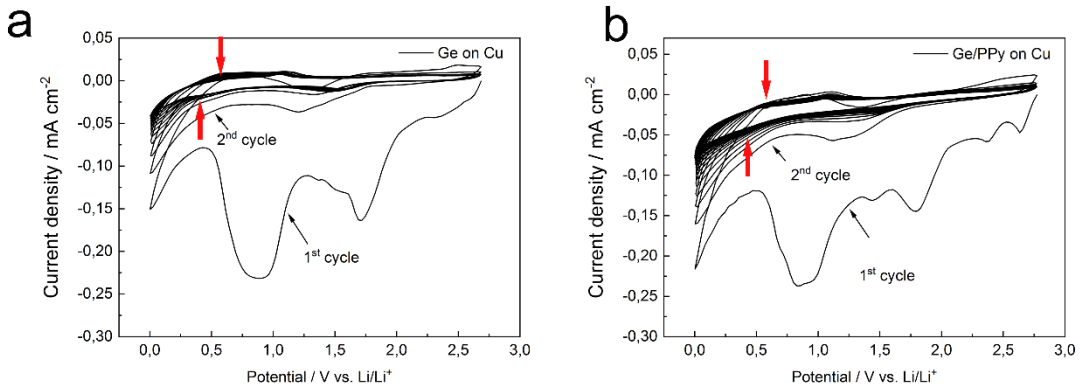

Figure 4 a) Cyclic voltammetry cycles recorded for 1 mol/L LiTFSI-[$Py_{1,4}$]TFSI on the electrodeposited Ge and b) on the Ge-PPy composite electrode. The scan rate was 10 mV s^{-1}.

Subsequently, galvanostatic charge-discharge cycles were performed at a current density of 0.15 A g^{-1}. Figure 5 compares the first charge/discharge curves of 1 mol/L LiTFSI-[$Py_{1,4}$]TFSI on the electrodeposited Ge (Ge/IL), Ge-PPy composite electrode (Ge-PPy/IL), and Ge with IL-PVdF-HFP polymer gel electrolyte (Ge/PVdF-IL). The specific capacities for lithiation were 1930 mAh g^{-1}, 1330 mAh $g^{-1,}$ and 1040 mAh g^{-1}, and the discharge capacities were 656 mAh g^{-1}, 851 mAh $g^{-1,}$ and 665 mAh g^{-1}, for Ge/IL, Ge-PPy/IL, and Ge/PVdF-IL, respectively. The Coulombic efficiencies recorded during the first charge-discharge cycle were approximately 34%, 64%, 64%, respectively. The irreversible capacity fading observed during the first cycle might be attributed to the irreversible Li insertion process, decomposition of the electrolyte, and the formation of the SEI.

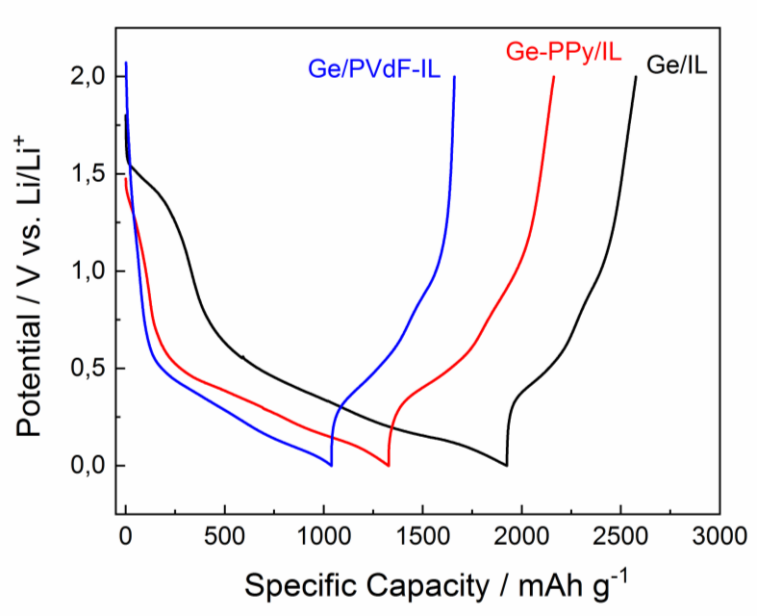

Figure 5 First galvanostatic charge-discharge capacity for Ge/IL, Ge-PPy/IL, and Ge/PVdF-IL at a current density 0.15 A g^{-1}.

These cells were cycled at ~0.3 C to compare the electrochemical performances observed during the charge-discharge cycles and study the process of SEI formation. The cell was first charged at a low current to activate the cell and then cycled at 0.3 C. The charge-discharge capacity and Coulombic efficiency of these cells are shown in Figure 6. In Figure 6a (red points), the initial discharge capacity is 480 mAh g^{-1} for Ge/IL, and the capacity decreases significantly during the subsequent cycles. After undergoing 13 discharge/charge cycles, the discharge capacity was recorded to be 400 mAh g^{-1} and the Coulombic efficiency improved from 90% to 97.3%. The cell maintained a discharge capacity of 266 mAh g^{-1} after 150 cycles. Figure 6a (black points) shows the discharge capacity of Ge-PPy/IL, which reduced from 560 mAh g^{-1} to 440 mAh g^{-1} over the first 20 cycles. In addition, the Coulombic efficiency oscillated during the first 20 cycles, which might be attributed to the formation of the unstable SEI. The PPy coating might have cracked, and fresh Ge_xLi or Ge phases could have been exposed to the electrolyte, which could have released Li or consumed Li to form the SEI. The discharge capacity faded to 285 mAh g^{-1} after 150 cycles. The Ge/PVdF-IL cell also exhibits a capacity fade, as shown in Figure 6a (blue points). The capacity gets reduced from 461 mAh g^{-1} to 200 mAh g^{-1} after 150 cycles. However, the Coulombic efficiency was quite stable at ~98%. It can be seen that Ge-PPy/IL has a higher discharge capacity than Ge/IL and the Ge/PVdF-IL polymer gel electrolytes in the Li|Ge cells. However, the voltage profiles in Figures 6b, 6c, and 6d do not present significant differences.

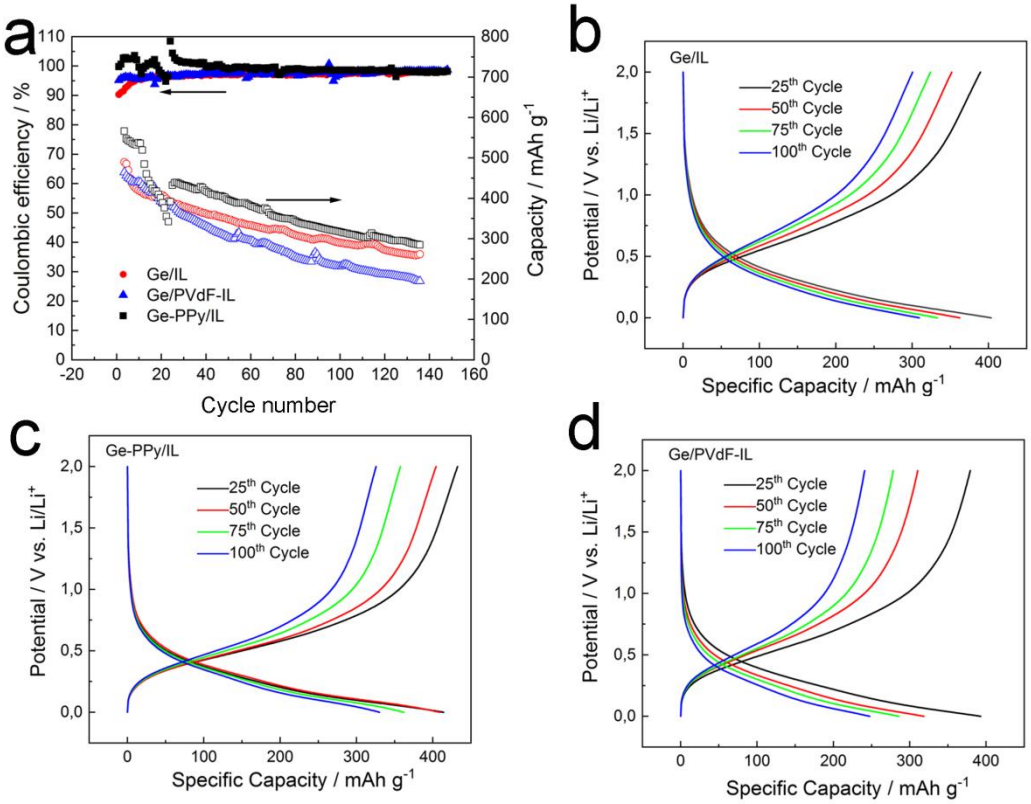

Figure 6 a) Charge-discharge capacity and Coulombic efficiency of Ge/IL, Ge-PPy/IL, and Ge/PVdF-IL at 0.3 C; Voltage profiles of b) Ge/IL, c) Ge-PPy/IL, and d) Ge/PVdF-IL, respectively.

3.3 SEI Analysis

The X-ray photoelectron spectroscopy (XPS) technique was used to evaluate the interfacial processes and the composition of the SEI after charge-discharge cycles. The survey spectral profiles recorded for the Ge/IL interphase after ~150 cycles are presented in Figure 7. The surfaces were etched under conditions of Ar sputtering to remove residual electrolytes. The XPS survey profiles primarily reveal the presence of decomposed ionic liquids products. The detailed spectral profiles of F 1s, N 1s, O 1s, C 1s, and S 2p were fitted to identify the components, and the results are shown in Figure 8. The binding energies of the components were calibrated using the C 1s peak appearing at 284.8 eV as a reference. Two F 1s peaks of significantly high intensity were observed in the spectral profile presented in Figure 8. The peak appearing at the high binding energy of 690.0 eV was assigned to the $TFSI^-$ anion, and the peak appearing at 686.5 eV was attributed to LiF. Three nitrogen peaks were present at 403.8 eV, 400.9 eV, and 399.5 eV, which were attributed to the $[Py_{1,4}]^+$ cation, $TFSI^-$ anion, and Li_3N, respectively, were observed in the N 1s profile. The $[Py_{1,4}]^+$ cation might also be decomposed by Li to form pyridine. This could potentially result in the generation of the N 1s peak at 400.9 eV. The O 1s profile presents a peak at 534.1 eV and a small peak at 531.8 eV, which were assigned to the $TFSI^-$ anion, and Li_2SO_3, respectively. The decomposition of the $TFSI^-$ anion results in the formation of SO_2 [37]. In the C 1s regime, four peaks were observed, which were attributed to the two CF_3 groups of the $TFSI^-$ anion (294.2 eV), C_{hetero} (288 eV), C_{alkyl} (286.6 eV), and adventitious carbon (284.8 eV). The peaks at 170.7 eV and 165.3 eV

in the S 2p spectrum were assigned to the $TFSI^-$ anion, and Li_2SO_3, respectively. The peak corresponding to Li 1s was weak, and this could be attributed to its relatively low sensitivity and the fact that it was partially covered by the electrolyte. It can be concluded from the results that the SEI of Ge/IL mainly consists of inorganic Li salts such as LiF, Li_2SO_3, Li_3N, and adsorbed and decomposed IL.

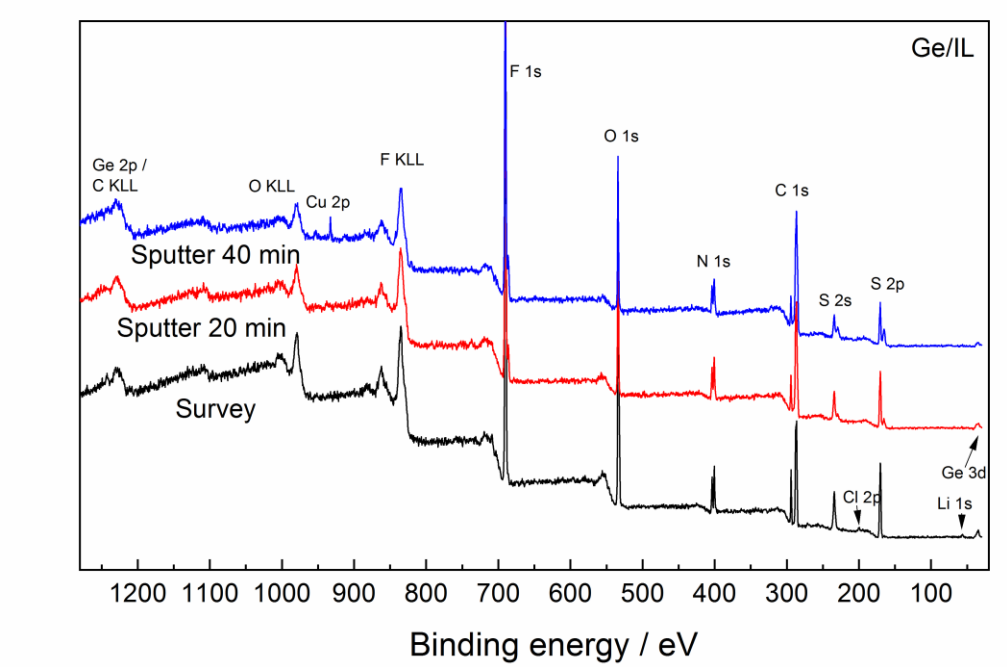

Figure 7 Survey spectral profiles recorded for the Ge/1 mol/L LiTFSI-$[Py_{1,4}]$TFSI interphase after 150 cycles (in the Li|Ge cell).

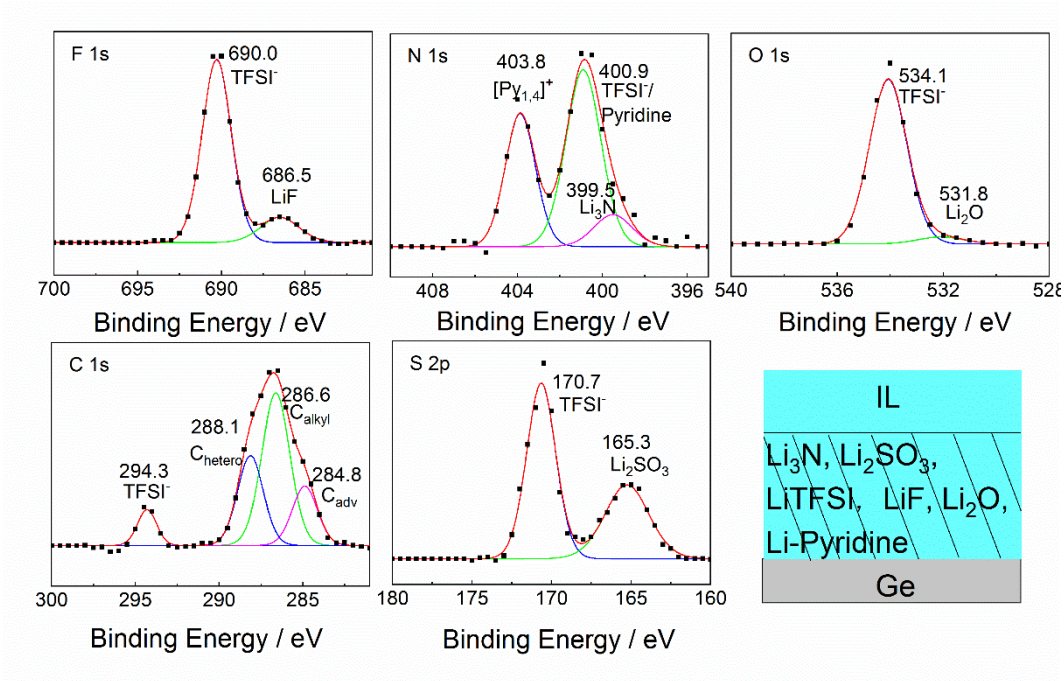

Figure 8 XPS profiles recorded for the F 1s, N 1s, O 1s, C 1s, and S 2p of the Ge (in 1 mol/L LiTFSI-$[Py_{1,4}]$TFSI electrolyte) interphase after 150 cycles (in the Li|Ge cell).

Figure 9 and Figure 10 display the XPS profiles recorded for the Ge-PPy/IL interphase after ~150 charge/discharge cycles. The survey spectral profiles in Figure 9 show the presence of Ge 2p and Ge 3d peaks, indicating that the SEI of the Ge-PPy/IL interphase is more compact than that of the Ge/IL interphase. The F 1s spectrum in Figure 10 reveals the presence of only one peak (at 686.0 eV). This was assigned to LiF. At the cycled Ge/PPy surface, signals of carbonate species (likely to be Li_2CO_3) were detected, as indicated by the O1s peak at 532 eV and C1s peak at 290.0 eV (not shown here). The presence of small amounts of Li_2O was indicated by the O 1s peak at 529.2 eV. The peaks at 169.9 eV and 162.5 eV in the S 2p regime can be attributed to $Li_2NS_2O_4$ and Li_2S, respectively. Analysis of the Ge 3d spectral profile reveals that the Ge surface is partly oxidized. The peak at 31.8 eV was assigned to GeO, and the one at 29.4 eV was attributed to elemental Ge. The reactivity of Li or the Ge/IL alloys (with the electrolyte) was largely suppressed by the PPy coatings. The SEI layer was compact and primarily consisted of inorganic Li salts.

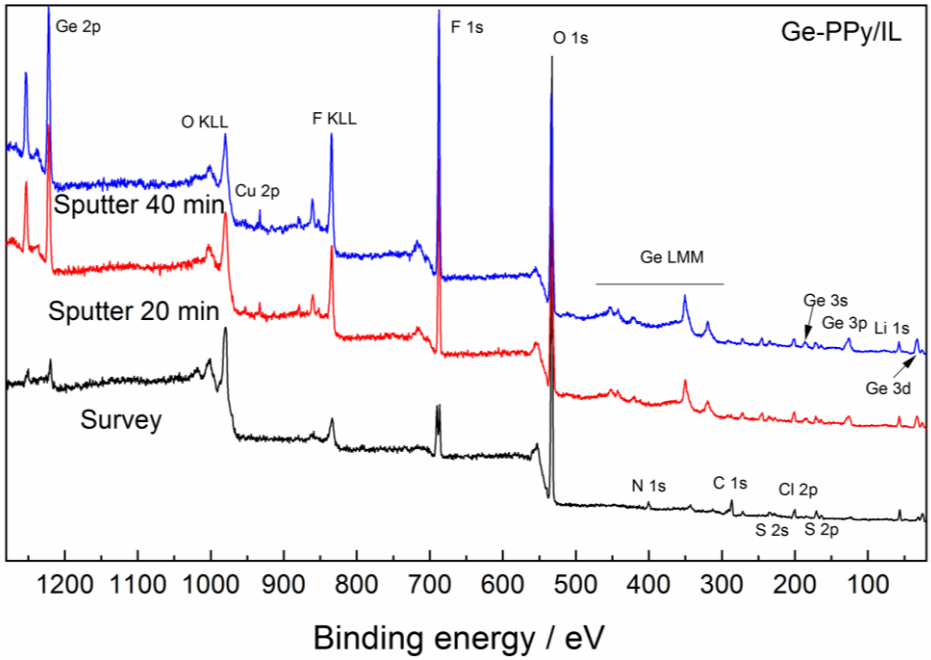

Figure 9 Survey spectral profiles recorded for the Ge-PPy/IL interphase after 150 cycles.

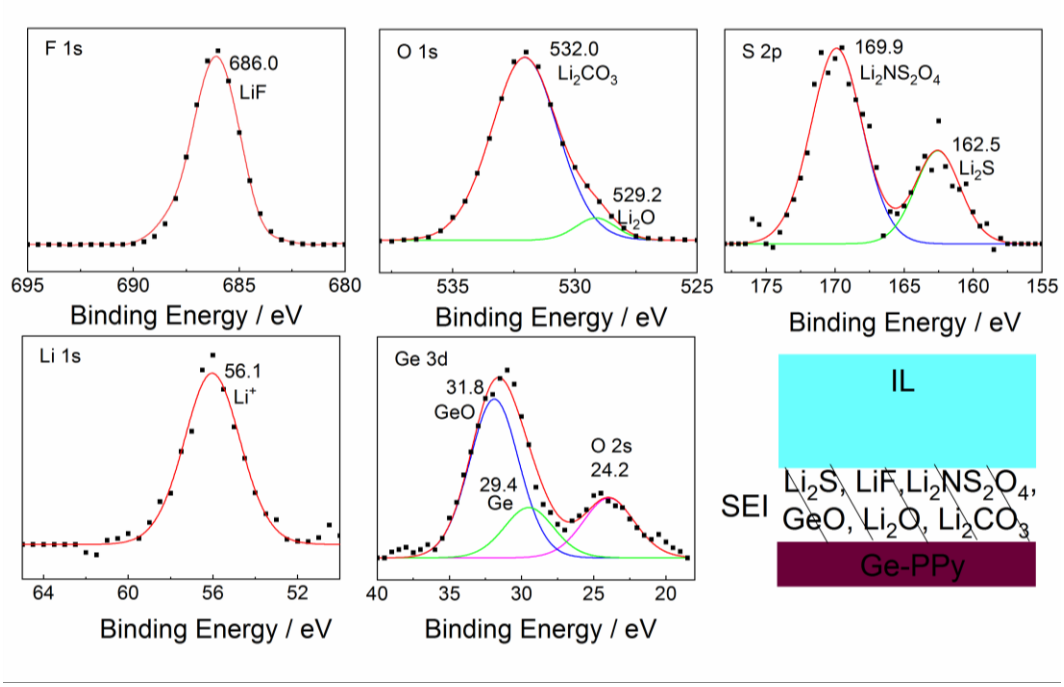

Figure 10 XPS profiles recorded for F 1s, O 1s, S 2p, Li 1s, and Ge 3d of the Ge-PPy/1 mol/L LiTFSI-[$Py_{1,4}$]TFSI interphase recorded after 150 cycles (in Li|Ge-PPy cell).

The XPS profiles recorded for the Ge/IL-PVdF polymer gel electrolyte interphase (in the Li|Ge cell) recorded after ~150 charge/discharge cycles are shown in Figure 11 and Figure 12. The compositions of the Ge/IL-PVdF polymer gel electrolyte interphase are quite similar to the compositions of the Ge-PPy/IL interphase. The SEI was compact and consisted of the decomposed products of LiF, Li_2S, Li_2CO_3, and $Li_2NS_2O_4$. However, the detected Ge 3d was completely oxidized, and this was validated by the presence of only two peaks at 33.0 eV and 31.0 eV in the Ge 3d spectral profile. These peaks were assigned to Ge_2O and GeO, respectively. This can potentially explain why Ge/IL-PVdF exhibits a reduced discharge capacity than Ge-PPy/IL.

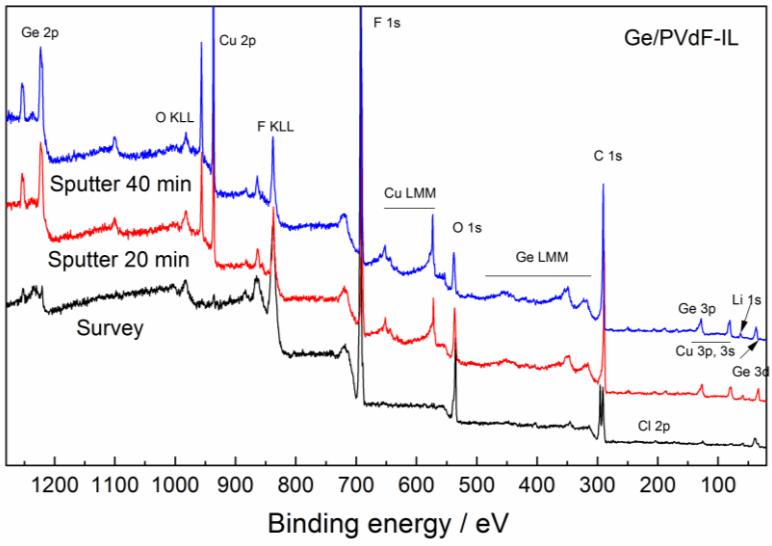

Figure 11 Survey spectral profile recorded for the Ge/IL-PVdF polymer gel electrolyte interphase after 150 cycles.

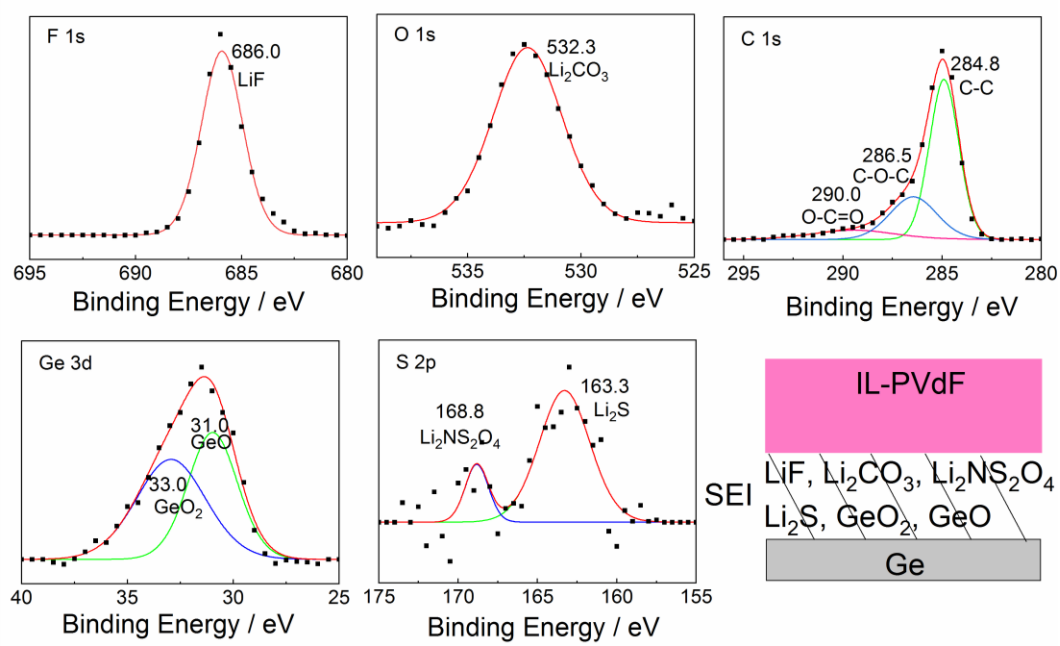

Figure 12 XPS profiles recorded for F 1s, O 1s, C 1s, Ge 3d, and S 2p of the Ge/1 mol/L LiTFSI-[Py1,4]TFSI electrolyte interphase after 150 cycles (in Li|Ge cell).

4. Conclusions

A composite Ge/polypyrrole (PPy) electrode was prepared for application in Li-ion batteries, and the composition of the SEI layer after charge/discharge was analyzed using the XPS technique. Ge particles (grain size: ~300 nm) were obtained following the process of electrodeposition using 0.2 mol/L of $GeCl_4$/[$Py_{1,4}$]TFSI. Polymerization was carried out using 0.05 mol/L of pyrrole/IL. The charge/discharge cycles were performed in 1 mol/L of LiTFSI/[$Py_{1,4}$]TFSI. The Ge-PPy composite electrode in IL-based electrolyte showed an initial capacity of 560 mAh g^{-1}, which was significantly higher than that of Ge in IL electrolyte (400 mAh g^{-1}) and that of Ge in the PVdF-IL polymer gel electrolyte (461 mAh g^{-1}). Although a significant extent of capacity fade can be observed in all Ge electrodes and Ge-PPy composite electrodes during the cycling process, Ge-PPy exhibited the maximum capacity retention of 285 mAh g^{-1} after 150 cycles. Meanwhile, the Ge-PPy composite electrode exhibited a stable Coulombic efficiency at approximately 98%. The interphases of the Ge/IL, Ge-PPy/IL, and Ge/Il-PVdF polymer gel electrolytes after 150 charge-discharge cycles were analyzed using the XPS technique. The results indicated the presence of a thick SEI layer primarily consisting of the decomposed $TFSI^-$ anion and absorbed IL present at the Ge/IL interphase. Compact SEI layers made of inorganic Li salts such as LiF, Li_2S, Li_2SO_3, and Li_2CO_3 were present at the Ge-PPy/IL and Ge/IL-PVdF interphases. It was inferred that PPy-coated Ge could effectively suppress the oxidation of Ge, resulting in a significant improvement in the discharge capacity.

Acknowledgments

The authors are grateful to S. Löffelholz for doing the scanning electron microscopy measurements.

Author Contributions

Conceptualization, Z.L. A.L. and F.E.; methodology, Z.L., A.L., Y.L., F.E.; investigation, Z.L., Y.L., A.L.; writing, reviewing and editing, Z.L, A.L., J.F.R. and F.E.; supervision, F.E. All authors have read and agreed to the published version of the manuscript.

Funding

We would like to thank Deutsche Forschungsgemeinschaft (DFG) (EN 370/28-1) for the funding. The ENABLES project has received funding from the European Union's Horizon 2020 research and innovation program, under Grant Agreement no. 730957.

Competing Interests

The authors have declared that no competing interests exist.

References

1. Nitta N, Wu F, Lee JT, Yushin G. Li-ion battery materials: Present and future. Mater Today. 2015; 18: 252-264.
2. Chu S, Cui Y, Liu N. The path towards sustainable energy. Nature Mater. 2017; 16: 16-22.
3. Lu J, Chen Z, Ma Z, Pan F, Curtiss LA, Amine K. The role of nanotechnology in the development of battery materials for electric vehicles. Nat Nanotechnol. 2016; 11: 1031-1038.
4. Gao X, Luo W, Zhong C, Wexler D, Chou SL, Liu HK, et al. Novel germanium/Polypyrrole composite for high power lithium-ion batteries. Sci Rep. 2014; 4: 6095.
5. Wu H, Cui Y. Designing nanostructured Si anodes for high energy lithium ion batteries. Nano Today. 2012; 7: 414-429.
6. Seng KH, Park MH, Guo ZP, Liu HK, Cho J. Self-assembled germanium/carbon nanostructured as high-power anode material for the lithium-ion battery. Angew Chem. 2012; 124: 5755-5759.
7. Kennedy T, Mullane E, Geaney H, Osiak M, O'Dwyer C, Ryan KM. High-performance germanium nanowire-based lithium-ion battery anodes extending over 1000 cycles through in situ formation of a continuous porous network. Nano Lett. 2014; 14: 716-723.
8. Li X, Yang Z, Fu Y, Qiao L, Li D, Yue H, et al. Germanium anode with excellent lithium storage performance in a germanium/lithium-cobalt oxide lithium-ion battery. ACS Nano. 2015; 9: 1858-1867.
9. Chockla AM, Klavetter KC, Mullins CB, Korgel BA. Solution-grown germanium nanowire anodes for lithium-ion batteries. ACS Appl Mater Interfaces. 2012; 4: 4658-4664.
10. Fuller CS, Severiens JC. Mobility of impurity ions in germanium and silicon. Phys Rev. 1954; 96: 21-24.
11. Tan LP, Lu Z, Tan HT, Zhu J, Rui X, Yan Q, et al. Germanium nanowires-based carbon composite as anode for lithium-ion batteries. J Power Sources. 2012; 206: 253-258.
12. Lahiri A, Borisenko N, Borodin A, Olschewski M, Endres F. Characterisation of the solid electrolyte interface during lithiation/delithiation of germanium in an ionic liquid. Phys Chem Chem Phys. 2016; 18: 5630-5637.
13. Liu XH, Liu Y, Kushima A, Zhang S, Zhu T, Li J, et al. In situ TEM experiments of electrochemical lithiation and delithiation of individual nanostructures. Adv Energy Mater. 2012; 2: 722-741.

14. Goriparti S, Miele E, De Angelis F, Di Fabrizio E, Proietti Zaccaria R, Capiglia C. Review on recent progress of nanostructured anode materials for li-ion batteries. J Power Sources. 2014; 257: 421-443.
15. Huo K, Wang L, Peng C, Peng X, Li Y, Li Q, et al. Crumpled n-doped carbon nanotubes encapsulated with peapod-like Ge nanoparticles for high-rate and long-life li-ion battery anodes. J Mater Chem A. 2016; 4: 7585-7590.
16. Li D, Wang H, Zhou T, Zhang W, Liu HK, Guo Z. Unique structural design and strategies for germanium-based anode materials toward enhanced lithium storage. Adv Energy Mater. 2017; 7: 1700488.
17. Luo W, Shen D, Zhang R, Zhang B, Wang Y, Dou SX, et al. Germanium nanograin decoration on carbon shell: Boosting lithium-storage properties of silicon nanoparticles. Adv Funct Mater. 2016; 26: 7800-7806.
18. Cho YJ, Im HS, Kim HS, Myung Y, Back SH, Lim YR, et al. Tetragonal phase germanium nanocrystals in lithium ion batteries. ACS Nano. 2013; 7: 9075-9084.
19. Park MH, Cho Y, Kim K, Kim J, Liu M, Cho J. Germanium nanotubes prepared by using the kirkendall effect as anodes for high-rate lithium batteries. Angew Chem Int Ed. 2011; 50: 9647-9650.
20. Fang S, Shen L, Zheng H, Zhang X. Ge-graphene-carbon nanotube composite anode for high performance lithium-ion batteries. J Mater Chem A. 2015; 3: 1498-1503.
21. Yang LC, Gao QS, Li L, Tang Y, Wu YP. Mesoporous germanium as anode material of high capacity and good cycling prepared by a mechanochemical reaction. Electrochem Commun. 2010; 12: 418-421.
22. Cheng XB, Zhang R, Zhao CZ, Wei F, Zhang JG, Zhang Q. A review of solid electrolyte interphases on lithium metal anode. Adv Sci. 2016; 3: 1500213.
23. An SJ, Li J, Daniel C, Mohanty D, Nagpure S, Wood DL. The State of understanding of the lithium-ion-battery graphite solid electrolyte interphase (SEI) and its relationship to formation cycling. Carbon. 2016; 105: 52-76.
24. Schroder K, Alvarado J, Yersak TA, Li J, Dudney N, Webb LJ, et al. The effect of fluoroethylene carbonate as an additive on the solid electrolyte interphase on silicon lithium-ion electrodes. Chem Mater. 2015; 27: 5531-5542.
25. Choi NS, Yew KH, Lee KY, Sung M, Kim H, Kim SS. Effect of Fluoroethylene carbonate additive on interfacial properties of silicon thin-film electrode. J Power Sources. 2006; 161: 1254-1259.
26. Yuan L, Wang J, Chew SY, Chen J, Guo ZP, Zhao L, et al. Synthesis and characterization of SnO2-polypyrrole composite for lithium-ion battery. J Power Sources. 2007; 174: 1183-1187.
27. Liu Q, Luo Y, Chen W, Yan Y, Xue L, Zhang W. CoP3@PPy Microcubes as anode for lithium-ion batteries with improved cycling and rate performance. Chem Eng J. 2018; 347: 455-461.
28. Liu J, Zhou W, Lai L, Yang H, Lim SH, Zhen Y, et al. Three dimensional α-Fe2O3/Polypyrrole (Ppy) nanoarray as anode for micro lithium ion batteries. Nano Energy. 2013; 2: 726-732.
29. Liu JX, Xu J, Chen YF, Sun WW, Zhou XX, Ke JH. Synthesis and electrochemical performance of a PEDOT:PSS@Ge composite as the anode materials for lithium-ion batteries. Int J Electrochem Sci. 2019; 14: 359-370.
30. Sun X, Lu X, Huang S, Xi L, Liu L, Liu B, et al. Reinforcing germanium electrode with polymer matrix decoration for long cycle life rechargeable lithium ion batteries. ACS Appl Mater. Interfaces 2017; 9: 38556-38566.

31. Endres F. Electrodeposition of a thin germanium film on gold from a room temperature ionic liquid. Phys Chem Chem Phys. 2001; 3: 3165-3174.
32. Meng X, Al-Salman R, Zhao J, Borissenko N, Li Y, Endres F. Electrodeposition of 3D ordered macroporous germanium from ionic liquids: A feasible method to make photonic crystals with a high dielectric constant. Angew Chem Int Ed. 2009; 48: 2703-2707.
33. Wu M, Vanhoutte G, Brooks NR, Binnemans K, Fransaer J. Electrodeposition of germanium at elevated temperatures and pressures from ionic liquids. Phys Chem Chem Phys. 2015; 17: 12080-12089.
34. Tylka MM, Willit JL, Williamson MA. Electrochemical nucleation and growth of uranium and plutonium from molten salts. J Electrochem Soc. 2017; 164: H5327-H5335.
35. Liu Z, Cui T, Pulletikurthi G, Lahiri A, Carstens T, Olschewski M, et al. Dendrite-free nanocrystalline zinc electrodeposition from an ionic liquid containing nickel triflate for rechargeable Zn-based batteries. Angew Chem Int Ed. 2016; 55: 2889-2893.
36. Agostini M, Sadd M, Xiong S, Cavallo C, Heo J, Ahn JH, et al. Designing a safe electrolyte enabling long-life Li/S batteries. ChemSusChem. 2019; 12: 4176-4184.
37. Alwast D, Schnaidt J, Hancock K, Yetis G, Behm RJ. Effect of Li+ and Mg2+ on the Electrochemical decomposition of the ionic liquid 1-butyl-1-methylpyrrolidinium bis (trifluoromethanesulfonyl)imide and related electrolytes. ChemElectroChem. 2019; 6: 3009-3019.